Journal of Power Sources, 40 (1992) 81–91

A model for simulating fast charging of lead/acid batteries

M. Maja, G. Morello and P. Spinelli
Department of Materials Science and Chemical Engineering, Polytechnical University of Turin, 10129 Turin (Italy)

Abstract

Among the various points which are discussed for the selection of batteries for electric vehicle applications, the possibility of fast charging is one of the most relevant. This is particularly true for the lead/acid battery which, at the present state of technology, must be charged at low rates to avoid serious shortening of its life. However, this type of battery can be successfully employed in electric vehicles for many advantageous features. The problems concerning some drawbacks of the lead/acid systems must be solved in order to improve its overall performance. In this paper we approached the problem of increasing the charging rate of the lead/acid battery by simulating, with a mathematical model, the discharge/charge conditions. Our aim was to derive useful information which could be applied to develop new technologies of fabrication. The simulations of the discharge/charge processes were carried out by studying the effect of different parameters such as plate dimensions, amount of acid, porosity of active masses and modality of charging. The results indicate that a significant increase of the charging rate can be obtained both by increasing the active mass porosity and by adopting adequate charging modalities.

Introduction

A key point in the use of storage batteries for electric vehicles is the possibility of their fast recharging. This is particularly true for lead/acid batteries which presently require to be charged at relatively low rates to avoid unacceptable shortening of their life which is caused mainly by local temperature increase, gas evolution, and grid corrosion.

In spite of this drawback, the lead/acid system still represents an excellent candidate for electric vehicle applications for many reasons. It presents advantageous features on one hand: low cost, ease of construction, solidity, expectance of improvement in the near future, and it does not seem to have competitors in the short term on the other hand. In fact, other systems technologically available as Ni–Cd have a higher cost and the so-called advanced systems, which certainly have attractive operating features, present various drawbacks and are not yet ready for commercialization.

Thus it is of great interest the investigation of possible solutions to the problem of significantly increasing the charging rate of the lead/acid battery, in order to develop new technologies of fabrication allowing the desired performances without a drastic increase of the cost.

We tried a first approach to this problem by developing a mathematical model capable to predict the behaviour of nonconventional lead/acid cells both on discharge and on charge by varying the characteristics of the active mass and the geometry of

0378-7753/92/$5.00

the cell. In the calculations presented here we started from literature data of the numerous parameters involved. Some of these parameters have been varied according to the requirements which are likely to be considered for electric vehicle applications.

The results have been evaluated by analysing the $V(t)$ curves computed for various conditions. Particularly we changed the charging current intensity, the charging modality (e.g., single or stepped), the porosity of the active mass, the thickness of the plates, and the amount of electrolyte.

The present paper reports the preliminary results obtained with the simulation and indicates the research line which we intend to pursue. From the indications of the mathematical model a set of experiments can be devised aiming both at the technological modifications and testing modalities in order to check the real behaviour of the improved system.

The model

Mathematical modelling of the lead/acid battery has been extensively treated in the past [1–12]. Different approaches have been used to predict the behaviour of both single plates and the complete cell. The major part of the models reported in the literature have the scope of predicting the behaviour of the battery during discharge and to compare the performance of different types of cells. Simulation of charging did not receive appreciable attention mainly because in the traditional utilization of the lead/acid cell the charging conditions are well defined and, when correctly applied, do not affect the discharge performance.

Our treatment is based on the macroscopic model according to the lines given by Newman and Tiedemann [1], and Simonsson [3] and has been partially developed in previous work [13, 14]. The basic approach is similar, but substantial improvements have been made [15], allowing a greater flexibility and extending the simulation to both discharging and charging.

The cell has been subdivided into four regions, (Fig. 1), corresponding to the porous lead electrode, the separator, the reservoir and the porous lead dioxide electrode. Each region can be given different geometrical (thickness) and physical (porosity, tortuosity) characteristics.

Starting from the basic materials balance equations, transport equations, and electrochemical kinetics equations the derivation of the set of simultaneous equations for the different regions has been obtained [15]. Some hints for the mathematical derivation are given in the appendix, a list of the symbols is also reported.

In our model we chose six explicit unknowns: sulfuric acid concentration c, velocity of solvent $\hat{v}_0$, molar flux of H^+ referred to the solvent $\hat{J}_1$, porosity ϵ, current density in the liquid $\hat{i}_L$, and overvoltage η.

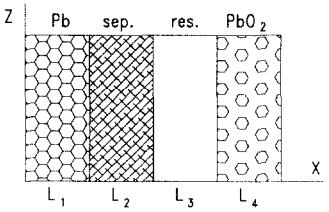

Fig. 1. One-dimensional model of the lead/acid cell subdivided into: lead electrode, separator, reservoir and lead dioxide.

For the two regions corresponding to the positive and negative electrodes, the following six simultaneous equations must be solved:

$$\epsilon \frac{\partial c}{\partial t} + \hat{v}_0 \frac{\partial c}{\partial x} + (1 - c\bar{V}_e) \frac{\partial \hat{J}_1}{\partial x} + \frac{(c\bar{V}_e - 1) + c\bar{V}_0 s_0}{nF} \frac{\partial \hat{i}_L}{\partial x} = 0 \tag{1}$$

$$\frac{\partial \hat{v}_0}{\partial x} + \bar{V}_e \frac{\partial \hat{J}_1}{\partial x} - \frac{\Delta V + \bar{V}_e s_1 + \bar{V}_0 s_0}{nF} \frac{\partial \hat{i}_L}{\partial x} = 0 \tag{2}$$

$$\hat{J}_1 = -\left(\epsilon D c \frac{\partial \ln a_\pm}{\partial c}\right) \frac{\partial c}{\partial x} + \frac{t_1 \hat{i}_L}{F} \tag{3}$$

$$\frac{\partial \epsilon}{\partial t} + \frac{\Delta V}{nF} \frac{\partial \hat{i}_L}{\partial x} = 0 \tag{4}$$

$$\left[\frac{1}{\epsilon\kappa} + \frac{1}{(1-\epsilon)\sigma}\right] \hat{i}_L - \frac{1}{(1-\epsilon)\sigma} i = \frac{\partial \eta}{\partial x} + \left[\frac{\partial \Delta\varphi}{\partial c} - \frac{RT}{F}(2t_1 - 1) \frac{\partial \ln a_\pm}{\partial c}\right] \frac{\partial c}{\partial x} \tag{5}$$

$$\frac{\partial \hat{i}_L}{\partial x} - a\Psi(c, \eta) = 0 \tag{6}$$

Equations (1), (2), and (4) reflect the materials balance in the liquid and in the solid. Equation (3) describes the mass transport in solution. Equation (5) states the conditions for charge transport as a consequence of both electric potential and chemical potential gradients. Equation (6) contains the electrochemical kinetics law.

For the reservoir and the separator regions, only the equations referring to the materials balance and transport in the liquid must be considered:

$$\epsilon \frac{\partial c}{\partial t} + \hat{v}_0 \frac{\partial c}{\partial x} + (1 - c\bar{V}_e) \frac{\partial \hat{J}_1}{\partial x} = 0 \tag{7}$$

$$\frac{\partial \hat{v}_0}{\partial x} + \bar{V}_e \frac{\partial \hat{J}_1}{\partial x} = 0 \tag{8}$$

$$\hat{J}_1 = -\left(\epsilon D c \frac{\partial \ln a_\pm}{\partial c}\right) \frac{\partial c}{\partial x} + \frac{t_1 \hat{i}_L}{F} \tag{9}$$

which contain the unknowns c, $\hat{v}_0$ and $\hat{J}_1$. A description of the symbols used in the above equations is given in the appendix.

After the solutions of the simultaneous equations for the various regions, according to the numerical method outlined below, the other variables of interest can be derived. Particularly the following can be obtained: the volume current $j = \partial \hat{i}_L / \partial x$, the current density in the solid $\hat{i}_S$, the faradic current $\hat{i}_F$, the electric potential in the solid φ_S and in the liquid φ_L from the following equations:

$$\frac{\partial \varphi_S}{\partial x} = -\frac{\hat{i}_S}{(1-\epsilon)\sigma} \tag{10}$$

$$\frac{\partial \varphi_L}{\partial x} = -\left[\frac{\hat{i}_L}{\epsilon\kappa} + \frac{RT}{F}(2t_1 - 1) \frac{\partial \ln a_\pm}{\partial c} \frac{\partial c}{\partial x}\right] \tag{11}$$

Thus, knowing the reversible potential difference $\Delta\varphi_{rev}$, the cell voltage can be obtained.

Other derived variables are: the volume fraction of sulphate y_4 and the degree of discharge X.

A set of boundary and initial conditions are given relating to the values of acid concentration and H^+ molar flux at the planes separating the various regions.

The numerical solutions of the above set of simultaneous equations is obtained by space discretization for every region: the first derivatives with respect to space are changed into finite differences by means of a three-node relationship. Thus, a set of equations containing total derivatives with respect to the time and algebraic equations is obtained which is discretized with respect to the time. An implicit discretization method was chosen for a better numerical stability. At this point the set of equations can be linearized and solved by means of the iterative Newton method.

The values of the chemical and physical parameters have been taken from the literature, e.g., partial molar volumes, diffusivity, transference numbers, electrolyte conductivity, electrolyte activity, conductivity of Pb, $PbSO_4$, and PbO_2, exchange-current density, reversible potentials [15].

In its present form, our model presents two limitations: one is the restriction to the one-dimensional treatment, the other is the isothermal conditions. Regarding the isothermal limitation, we can use our model for calculations at different temperatures, at least for the known data referring to the temperature dependence of the above parameters, but we cannot account for temperature variation during cell operation. This is of course of primary importance when charging and discharging the battery at high rates.

We plan to overcome both limitations in future work. The extension to a bi-dimensional treatment does not involve a large mathematical revision; on the contrary, the temperature dependence requires a new mathematical description with a significant increase of numerical difficulty and computational time.

Results and discussion

Some of the simulated results are presented in this section. We included some simulations of discharge for a better understanding of the discussion regarding the change of initial porosity, i.e., the porosity of the unused, completely charged plate.

Figure 2 reports the cell voltage versus time during discharge at different rates. If we plot some of the calculated variables for increasing discharge times, we obtain an interesting picture of the cell behaviour. As an example we have reported in Figs. 3 and 4 the acid concentration profiles and the degree of discharge profiles at various times for a discharge rate of 500 A m^{-2}. It can be observed that with this rather high discharge rate, the utilization of the active mass is not very good, and concentration limitations set up very soon.

In order to discuss the possibility of improving the battery performance, we tried to simulate a change of the active mass porosity. For a correct comparison of the results referring to different porosity values, we chose to fix the thickness of the electrodes and according to the porosity value we varied the surface area of the electrodes in order to obtain the same amount of active mass. This type of calculation has been carried out both on discharge and charge.

Figure 5 illustrates the values of the cell capacity as a function of the discharge current for different values of the initial porosity in the range 0.4 to 0.8. The calculation has been done with the following conditions: thickness of positive and negative active mass 1 mm; thickness of electrolyte 2 mm without separator; the discharge current

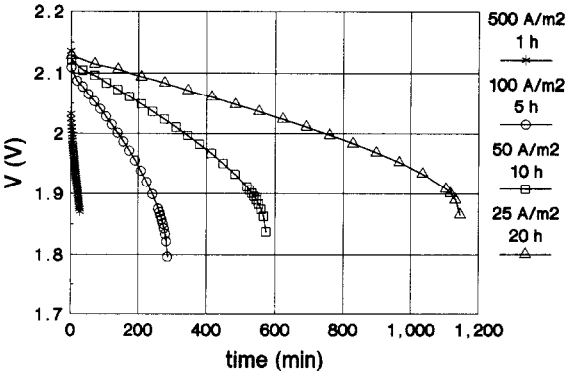

Fig. 2. Computed discharge curves at different rates.

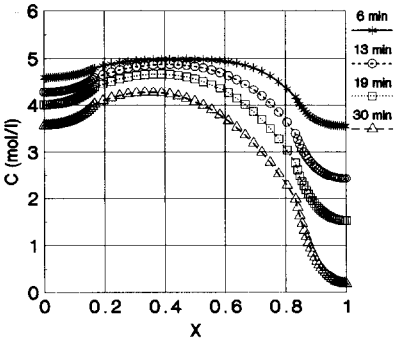

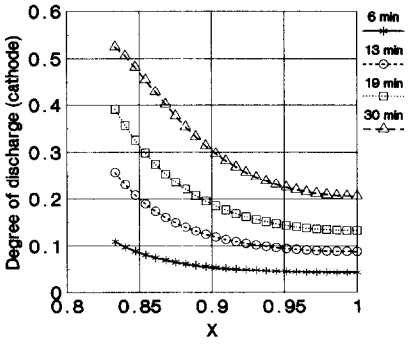

Fig. 3. Concentration profiles for different discharge times at $I=500$ A. The cell capacity is 450 A h. The nondimensional abscissa X corresponds to 1 mm anode, 4 mm electrolyte, 1 mm cathode.

Fig. 4. Degree of discharge within the cathodic mass for different discharge times; see Fig. 3.

is referred to 1 m^2 of electrode for a porosity value of 0.6; when the porosity is changed, the electrode area is varied in the amount required to have the same mass of active materials. The choice relating to the thickness of the various regions was determined by the fact that we intended to study discharge conditions limited by the positive electrode. For the data reported in Fig. 5, the amount of positive active mass was 3750 g and the limiting value of the capacity was 451 A h, assuming a utilization coefficient of 0.55 for the positive active mass. This gives 8.3 g of PbO_2 per A h which is very close to the standard value employed in starting-lighting-and-ignition (SLI) batteries. We can see that the capacity/current profile is a typical 'S' shaped curve. At low currents the capacity tends to the theoretical value given by the amount of active mass corrected for the utilization coefficient. When the current increases, the capacity rapidly decreases with a strong dependence on the porosity.

It is interesting to note that a remarkable influence of porosity on the capacity is observed in the range 250 to 500 A m^{-2} corresponding, for the above reported conditions, to a very high discharge rate ($C/2$, $C/1$). For rates below $C/5$, the change of capacity with porosity is very small.

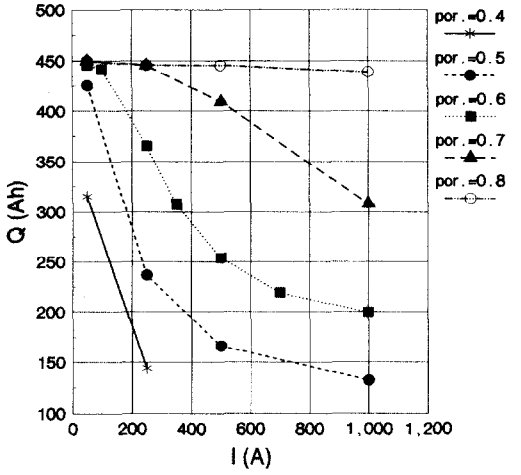

Fig. 5. Capacity of the modelled cell vs. current intensity for various values of the initial porosity of the active masses.

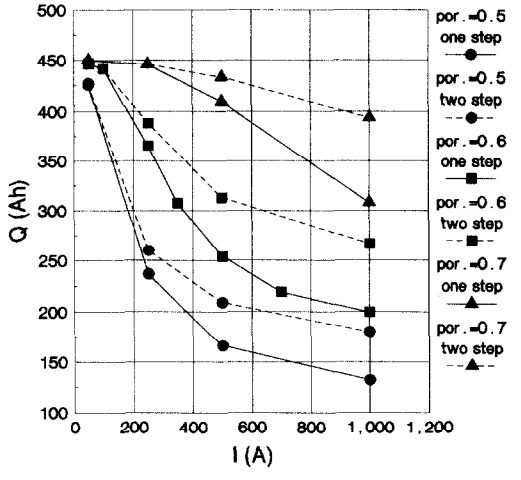

Fig. 6. Capacity of the modelled cell vs. current intensity for various values of the initial porosity of the active masses. Solid lines refer to one-step discharge, dashed lines refer to two-step discharge.

In order to simulate different discharge modalities, we calculated the battery capacity for a two-step discharge. A first step-up to 70% of the nominal capacity, then, after a rest, necessary to restore a uniform acid concentration, a second step with the same current. The total capacity was the sum of the charges involved in each step. As one might expect, we observed a beneficial effect in the sense that the two-step capacity was always greater than the corresponding one-step capacity. What is interesting to note is that, Fig. 6, this benefit significantly increases with increasing the discharge current and strongly depends on the porosity value. The per cent increment of the capacity obtained with a two-step discharge is shown in Fig. 7 as a function of the discharge current, for three porosity values.

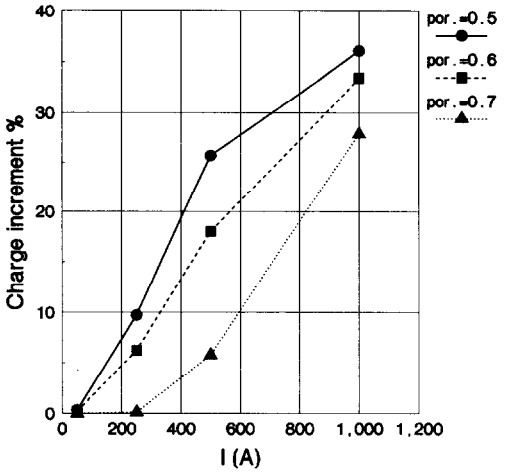

Fig. 7. Increment of the capacity obtained by a two-step discharge vs. current intensity, for various initial porosity values.

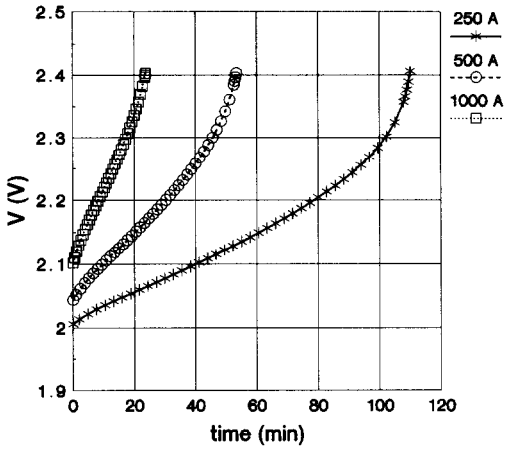

Fig. 8. Charging curves at different rates for an initial (before the discharge) porosity of 0.7.

The simulation of the charging requires some preliminary comment. We thought of testing our model by a simple cycle consisting of a slow discharge (20 h) followed by a rest and then the charge at the desired rate (2, 1, 0.5 h). The values of porosity refer to the initial porosity at the beginning of the cycle. At the end of the charge, the average porosity may differ from the initial value depending on the charging rate.

Figure 8 illustrates the charging curves at three rates for an initial porosity of 0.7, whereas Fig. 9 illustrates the effect of a two-step charging. We used the same modality as for the discharge, i.e., a first step-up to 70% of the nominal capacity and then the second step.

It can be observed that also on charging a beneficial effect is obtained, in terms of total capacity, with a two-step modality. However, if we look at the values, the

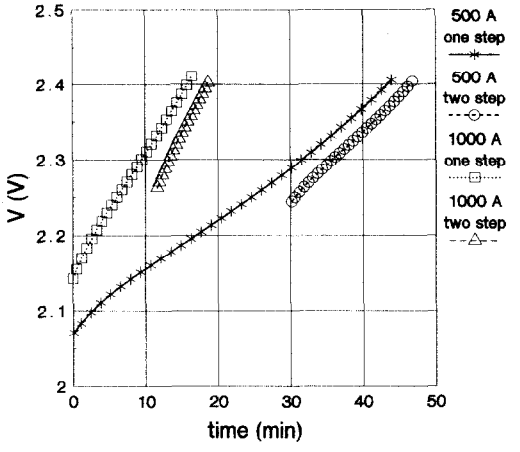

Fig. 9. Two-step charging at different rates for an initial (before the discharge) porosity of 0.6. The first step ended at about 70% of the nominal capacity.

benefit is lower compared with the discharge condition. This is due to the reciprocal duration of the two steps. To enhance the charge acceptance we have to choose a first step of smaller duration, because the advantage of restoring a uniform acid concentration during the rest time can be greater when the average concentration is small.

Conclusion

The preliminary data that we have illustrated in the previous section indicate that our mathematical model can be satisfactorily employed to study the charging of the lead/acid battery.

The analysis of the results has shown that to increase the charging rate, in view of electric vehicle applications, two possible actions can be undertaken: (i) increasing the porosity of the active masses, and (ii) step charging.

The beneficial effect of step charging decreases at high porosities when the sulfuric acid is mainly contained in the porous masses. This consideration indicates that the use of gelled electrolyte could introduce further advantages, this situation can also be simulated by the proposed model.

Technological problems can presently limit the possibility of increasing the active mass porosity, particularly for the positive plate. This indicates the need to undertake an extensive experimental action for characterizing non traditional supporting materials and for improving the soundness of the plates at high porosities.

The goal of these studies is to ascertain the economical compatibility of improved lead/acid batteries compared with other alternative systems.

Appendix

The following is not a complete mathematical derivation of eqns. (1–6). We only present here some hints which can help in reconstructing the whole treatment.

By proper definition of the stoichiometric coefficients, the electrochemical reactions can be generalized in the following form:

$$s_0H_2O + s_1H^+ + s_2HSO_4^- + s_3Pb + s_4PbSO_4 + s_5PbO_2 + ne = 0$$

Table 1 reports the values of the coefficients for the discharge conditions. On charge, the sign of all the coefficients must be reversed.

Indexes $i=0$, 1, 2 refer to species in solution, whereas indexes $j=3$, 4, 5 refer to species in the solid.

In order to derive eqns. (1)–(4), we start from the basic equations for the materials balance in the liquid:

$$\frac{\partial \epsilon c_i}{\partial t} + \frac{\partial \epsilon N_i}{\partial x} = \frac{s_i}{nF} j \tag{12}$$

and in the solid:

$$\frac{\partial (1-\epsilon) c_j}{\partial t} = \frac{s_j}{nF} j \tag{13}$$

If we refer to the species H^+ ($i=1$), recalling the definitions of the molar flux $N_1 = c_1 v_1$ and the molar flux respect to the solvent $J_1 = c_1(v_1 - v_0)$, substituting $N_1 = c_1 v_0 - J_1$ into the previous equations, being $c_1 = c_2 = c$, after some rearrangements and taking into account the Gibbs–Duhem relationship, the following equations are obtained:

$$\frac{\partial \epsilon c}{\partial t} + \frac{\partial \epsilon (c v_0 + J_1)}{\partial x} = \frac{s_1}{nF} j \tag{14}$$

$$\frac{\partial \epsilon c_0}{\partial t} + \frac{\partial \epsilon c_0 v_0}{\partial x} = \frac{s_0}{nF} j \tag{15}$$

$$\frac{\partial \epsilon}{\partial t} = -\frac{1}{nF} j \sum_j \bar{V}_j s_j \tag{16}$$

By introducing the partial molar volumes for the electrolyte $\bar{V}_e = \bar{V}_1 + \bar{V}_2$ and for the solvent $\bar{V}_0$, after some rearrangements, eqns. (1), (2) and (4) are obtained.

Equation (3) is one of the basic transport equations in solution and is easily derived. Equation (5) can be obtained by considering the charge-transport equation in solution:

TABLE 1

Stoichiometric coefficients for the electrochemical reactions under discharge

Index	Species	Cathode	Anode
$i=0$	H_2O	$s_0 = +2$	$s_0 = 0$
$i=1$	H^+	$s_1 = -3$	$s_1 = +1$
$i=2$	HSO_4^-	$s_2 = -1$	$s_2 = -1$
$j=3$	Pb	$s_3 = 0$	$s_3 = -1$
$j=4$	$PbSO_4$	$s_4 = +1$	$s_4 = +1$
$j=5$	PbO_2	$s_5 = -1$	$s_5 = 0$
	e	$n = -2$	$n = +2$

$$i_L = -\kappa \frac{\partial \varphi_L}{\partial x} - \frac{\kappa RT}{F}(2t_1 - 1) \frac{\partial \ln a_\pm}{\partial c} \frac{\partial c}{\partial x} \tag{17}$$

together with the following relationships:

$$\hat{i}_L + \hat{i}_S = i$$

$$\hat{i}_S = i_S(1 - \epsilon)$$

$$i_S = -\sigma \frac{\partial \varphi_S}{\partial x}$$

$$\varphi_S - \varphi_L = (\Delta\varphi_L^S)_{rev} + \eta$$

$$\frac{\partial \varphi_S}{\partial x} - \frac{\partial \varphi_L}{\partial x} = \frac{\partial \eta}{\partial x} + \frac{\partial (\Delta\varphi_L^S)_{rev}}{\partial x}$$

Equation (6) contains the electrochemical kinetics expression, which has been assumed to be the Butler–Volmer equation:

$$\Psi(c, \eta) = i_0 \left[\exp\left(\alpha_a \frac{F\eta}{RT} \right) - \exp\left(-\alpha_c \frac{F\eta}{RT} \right) \right] \tag{18}$$

This expression provides the value of the faradic current density i_F. The amount of charge transferred between the solid and the liquid per unit of time and volume is $j = ai_F$, a being the electrochemical active area per unit of electrode volume. This last quantity can be related to the degree of reaction X:

$$a = a^0 \left(1 - \frac{X}{X_M} \right) \tag{19}$$

where a^0 is the initial value of the active area and X_M the maximum degree of reaction (discharge or charge).

Some other points should be mentioned. The solid conductivity σ is a function of the volume fraction of sulfate and tortuosity in addition to the contribution of the intrinsic conductivities σ_j of the components. The correlation among these quantities has been obtained according to the indications by Metzendorf [16].

The diffusivity of the electrolyte D has been corrected by the tortuosity factor, which has been presently introduced as a simple coefficient, but it could be improved on the basis of a refined approach [17].

List of symbols

α_a, α_c	charge transfer coefficients
ΔV	volume change in the solid phase, $m^3\ mol^{-1}$
ϵ	porosity
η	overvoltage, V
κ	conductivity of liquid, $\Omega^{-1}\ m^{-1}$
σ	conductivity of solid, $\Omega^{-1}\ m^{-1}$
φ_L, φ_S	Galvani potential in the liquid, solid, V
a	elecrochemical active area per unit of electrode volume, m^{-1}
$a_\pm$	mean ionic activity
c	sulfuric acid concentration, mol m^{-3}

c_i molar concentration of species i, mol m^{-3}
D electrolyte diffusivity, m^2 s^{-1}
F Faraday's constant, C mol^{-1}
i total current density referred to the electrode area, A m^{-2}
i_F faradic current density referred to the a area, A m^{-2}
i_0 exchange current density, A m^{-2}
i_L current density in the liquid referred to the section area of the liquid, A m^{-2}
$\hat{i}_L$ current density in the liquid referred to the section area of the electrode, A m^{-2}
i_S, $\hat{i}_S$ current density in the solid (as above), A m^{-2}
$\hat{J}_1$ molar flux of H^+ referred to the solvent, mol m^{-2} s^{-1}
j electric charge transferred between solid and liquid per unit of time and per unit of electrode volume, A m^{-3}
N_i molar flux of species i, mol m^{-2} s^{-1}
n number of electrons involved in the reactions
R universal gas constant, J mol^{-1} K^{-1}
s_i, s_j stoichiometric coefficients of species i, j
T temperature, K
t time coordinate, s
t_i transference number of species i
$\hat{v}_0$ velocity of solvent, m s^{-1}
$\bar{V}_i$, $\bar{V}_j$ partial molar volume of species i, j, m^3 mol^{-1}
$\bar{V}_e$ partial molar volume of electrolyte, m^3 mol^{-1}
$\bar{V}_0$ partial molar volume of solvent, m^3 mol^{-1}
X degree of reaction (charge or discharge)
x space coordinate, m
y_j volume fraction of species j in the solid

References

1 J. Newman and W. Tiedemann, *AIChE J., 21* (1975) 25.
2 W. Tiedemann, J. Newman, in S. Gross, (ed.), *Battery Design and Optimization,* The Electrochemical Society, Pennington, NJ, 1979, p. 23.
3 D. Simonsson, *J. Appl. Electrochem., 3* (1973) 261.
4 D. Simonsson, *J. Appl. Electrochem., 4* (1974) 109.
5 K. Micka and I. Rousar, *Electrochim. Acta, 18* (1973) 629.
6 K. Micka and I. Rousar, *Electrochim. Acta, 19* (1974) 499.
7 K. Micka and I. Rousar, *Electrochim. Acta, 21* (1975) 599.
8 W. G. Sunu and B. W. Burrows, *J. Electrochem. Soc., 128* (1981) 1405.
9 W. G. Sunu and B. W. Burrows, *J. Electrochem. Soc., 129* (1982) 688.
10 W. G. Sunu and B. W. Burrows, *J. Electrochem. Soc., 131* (1984) 1.
11 Hiram Gu and T. V. Nguyen, *J. Electrochem. Soc., 134* (1987) 2953.
12 E. C. Dimpault-Darcy, T. V. Nguyen and R. E. White, *J. Electrochem. Soc., 135* (1988) 278.
13 G. Morello, *Thesis,* University of Turin, Turin, Italy, 1985.
14 M. Maja and P. Spinelli, *J. Power Sources, 30* (1990) 201.
15 G. Morello and P. Spinelli, Private communication.
16 H. Metzendorf, *J. Power Sources, 7* (1982) 281.
17 J. Bear, *Dynamic of Fluids in Porous Media,* Elsevier, Amsterdam/New York, 1972.